^{99m}Tc-Macroaggregated Albumin Poorly Predicts the Intrahepatic Distribution of ^{90}Y Resin Microspheres in Hepatic Radioembolization

Maurits Wondergem, Maarten L.J. Smits, Mattijs Elschot, Hugo W.A.M. de Jong, Helena M. Verkooijen, Maurice A.A.J. van den Bosch, Johannes F.W. Nijsen, and Marnix G.E.H. Lam

Department of Radiology and Nuclear Medicine, UMC Utrecht, Utrecht, The Netherlands

In hepatic ^{90}Y radioembolization, pretreatment ^{99m}Tc-macroaggregated albumin (^{99m}Tc-MAA) nuclear imaging is used for lung shunt analysis, evaluation of extrahepatic deposition, and sometimes for treatment planning, using a partition model. A high level of agreement between pretreatment ^{99m}Tc-MAA distribution and final ^{90}Y-microsphere distribution is assumed. The aim of this study was to investigate the value of pretreatment ^{99m}Tc-MAA SPECT to predict intrahepatic posttreatment ^{90}Y-microsphere distribution. **Methods:** Volumes of interest (VOIs) were delineated on pretreatment contrast-enhanced CT or MR images according to Couinaud liver segmentation. All VOIs were registered to the ^{99m}Tc-MAA SPECT and ^{90}Y SPECT images. The ^{99m}Tc-MAA SPECT and ^{90}Y SPECT activity counts were normalized to the total administered activity of ^{90}Y. For each VOI, this practice resulted in a predictive amount of ^{90}Y (MBq/cm^3) based on ^{99m}Tc-MAA SPECT in comparison with an actual amount of ^{90}Y based on ^{90}Y SPECT. Bland–Altman analysis was used to investigate the agreement of the activity distribution between ^{99m}Tc-MAA SPECT and ^{90}Y SPECT. **Results:** A total of 39 procedures (225 VOIs) in 31 patients were included for analysis. The overall mean difference between pretreatment and posttreatment distribution of activity concentration for all segments was −0.022 MBq/cm^3 with 95% limits of agreement of −0.581 to 0.537 MBq/cm^3 (−28.9 to 26.7 Gy absorbed dose). A difference of >10%, >20%, and >30% of the mean activity per milliliter was found in, respectively, 153 (68%), 97 (43%), and 72 (32%) of the 225 segments. In every ^{99m}Tc-MAA procedure, at least 1 segment showed an under- or overestimation of >10%. The position of the catheter tip during administrations, as well as the tumor load of the liver segments, significantly influenced the disagreement. **Conclusion:** In current clinical practice, ^{99m}Tc-MAA distribution does not accurately predict final ^{90}Y activity distribution. Awareness of the importance of catheter positioning and adherence to specific recommendations may lead to optimization of individualized treatment planning based on pretreatment imaging.

Key Words: ^{99m}Tc-MAA; ^{90}Y microspheres; radioembolization; dosimetry; liver

J Nucl Med 2013; 54:1294–1301
DOI: 10.2967/jnumed.112.117614

Radioembolization with ^{90}Y microspheres is widely used for treatment of primary or metastatic liver malignancies. Selective injection of these microspheres in the hepatic artery results in high absorbed tumor doses while largely sparing the surrounding normal liver parenchyma, which is dependent mainly on the portal vein for its blood supply (*1–3*).

In a pretreatment angiographic procedure the anatomy of the liver vasculature is evaluated, and hepaticoenteric anastomoses that may lead to extrahepatic deposition of activity are occluded by coil embolization (*4*). Thereafter ^{99m}Tc-macroaggregated albumin particles (^{99m}Tc-MAA) are injected in the liver artery supplying the target volume, and the distribution of ^{99m}Tc-MAA is visualized by scintigraphy. Most centers that perform radioembolization use the distribution of ^{99m}Tc-MAA to calculate the lung shunt fraction and to detect any extrahepatic deposition of activity (*5,6*). Furthermore, it is assumed that ^{99m}Tc-MAA can also be used to predict the intrahepatic distribution of ^{90}Y-microspheres, and as such, ^{99m}Tc-MAA is sometimes used for individualized treatment planning by the so-called partition model (*7–9*).

In most of the patients, the prescribed activities for radioembolization are calculated with methods based on liver weight or on a combination of body surface area and tumor liver involvement (*10*). The absorbed dose to the tumor and any accompanying toxicity effects to the normal liver parenchyma may be observed only after the actual treatment. Dosimetry can be used for individualized treatment planning and aims to optimize treatment efficacy with acceptable toxicity. Pretreatment dosimetry, however, requires a scout or safety dose as a reference for the treatment, for example by using the ^{99m}Tc-MAA distribution as a reference for posttreatment dose distribution.

The partition model is suggested as an alternative means of activity calculation in patients with a limited number of hypervascular liver tumors, optimizing the administered activity in individual patients (*5*). Tumor-to-nontumor activity ratios on pretreatment ^{99m}Tc-MAA SPECT are used to calculate activities that better reflect the intrahepatic dose distribution. In clinical practice, this means that the partition-model–based activity may be much higher than prescribed activities that are based on the more conventional methods, especially in patients with hypervascular tumors, having high tumor-to-nontumor activity ratios (*11*).

The partition model relies on ^{99m}Tc-MAA as a predictor for ^{90}Y-microsphere distribution. However, the predictive value of ^{99m}Tc-MAA for the distribution of ^{90}Y-microspheres in the liver is still a matter of debate (*12*). Parameters that may influence

Received Nov. 23, 2012; revision accepted Mar. 12, 2013.
For correspondence or reprints contact: Marnix Lam, Department of Radiology and Nuclear Medicine, University Medical Center Utrecht, Heidelberglaan 100, 3584 CX Utrecht, The Netherlands.
E-mail: m.lam@umcutrecht.nl
Published online Jun. 7, 2013.
COPYRIGHT © 2013 by the Society of Nuclear Medicine and Molecular Imaging, Inc.

distribution differences between ^{99m}Tc-MAA and ^{90}Y-microspheres include interval differences in catheter position, physiologic variances in hepatic blood flow, size and morphology differences between ^{99m}Tc-MAA particles and ^{90}Y-microspheres, tumor histopathology, and tumor load. These and other factors may all limit the agreement between ^{99m}Tc-MAA and ^{90}Y-microsphere distribution.

The aim of this study was to investigate the value of ^{99m}Tc-MAA to predict ^{90}Y-microsphere distribution. Insight on this matter is essential for further development of any dose calculation method based on pretreatment ^{99m}Tc-MAA distribution.

MATERIALS AND METHODS

Patients

All patients who were treated with radioembolization from the start of our program in February 2009 up to February 2012 were retrospectively analyzed. The institutional review board approved this study and waived the requirements for patient informed consent. Patients who had received both the pretreatment administration of ^{99m}Tc-MAA and the treatment with ^{90}Y-microspheres were included. Exclusion criteria were missing data, malregistration of imaging data, and procedures with multiple administrations, rendering it impossible to relate individual administrations to specific target volumes. In some patients, 2 separate lobar procedures were included in the study analysis. Subsegmental administrations were not performed.

Radioembolization

All procedures were performed according to international consensus (*13*). In short, during a pretreatment angiographic procedure, a 5-French catheter was used to evaluate hepatic vascular anatomy and to identify nontarget vessels leading to organs other than the liver. In general, the gastroduodenal artery and the right gastric artery were coil-embolized to prevent extrahepatic deposition of activity. Any other vessels branching off near the injection site and leading to nontarget organs were embolized as well. The cystic artery was not prophylactically embolized. Consecutively, a scout dose of ^{99m}Tc-MAA (150 MBq, 0.8 mg in 3.0 mL, TechneScan LyoMaa; Mallinckrodt Medical B.V.) was injected via a slow-pulsed injection, followed by planar imaging and SPECT, to check for inadvertent extrahepatic deposition. ^{99m}Tc-MAA was prepared immediately before administration; imaging was performed immediately after administration. If the ^{99m}Tc-MAA was not distributed to any nontarget area (including a hepatopulmonary shunt $\leq$ 20%), the patient was scheduled for treatment (mean interval, 12 d; range, 0–23 d). However, in the case of inadvertent ^{99m}Tc-MAA distribution, a second pretreatment procedure was performed to embolize the culprit vessels. In those cases, only the most recent ^{99m}Tc-MAA SPECT study was used for analyses. No vessels were coil-embolized after final ^{99m}Tc-MAA administration. Resin microspheres (SIR-Spheres; Sirtex) were used for treatment. Activity calculations were based on the body surface area method (prescribed activity in GBq, body surface area – 0.2 + fractional tumor involvement). Patients with a lung shunt fraction of >20% were excluded from treatment, and in patients with a lung shunt fraction of 10%–15% or 15%–20% a reduction of 20% and 40% was applied, respectively. Per protocol, the interventional radiologist placed the catheter tip in the same position during both procedures. The microspheres were infused slowly, with intermittent contrast injection and digital subtraction angiography to check for stasis. All administered activity was corrected for any residual activity after treatment.

Imaging

Pre- and posttreatment imaging was performed on a dual-head γ-camera (Forte [Philips] for 7 procedures and Symbia [Siemens Health Care] for 32 procedures). Pretreatment ^{99m}Tc-MAA planar and SPECT images were acquired on a 128 × 128 matrix using a 129.5- to 150.5-keV energy window and a low-energy general-purpose collimator. For posttreatment ^{90}Y bremsstrahlung SPECT imaging, the combination of a high-energy general-purpose collimator and a wide 50- to 250-keV energy window was used, which yields images with a favorable combination of sensitivity and contrast (*14*). SPECT imaging was performed with 120 projections over a noncircular orbit of 180° (Forte; 30 s/projection) or 360° (Symbia; 20 s/projection). Data were reconstructed using ordered-subsets expectation maximization (5 iterations, 8 subsets) including attenuation correction and a gaussian postreconstruction filter of 5 mm in full width at half maximum. The reconstructed voxel size was 4.7 × 4.7 × 4.7 mm, 3.9 × 3.9 × 3.9 mm, and 4.8 × 4.8 × 4.8 mm, for Forte images, Symbia ^{99m}Tc-MAA images, and Symbia ^{90}Y images, respectively.

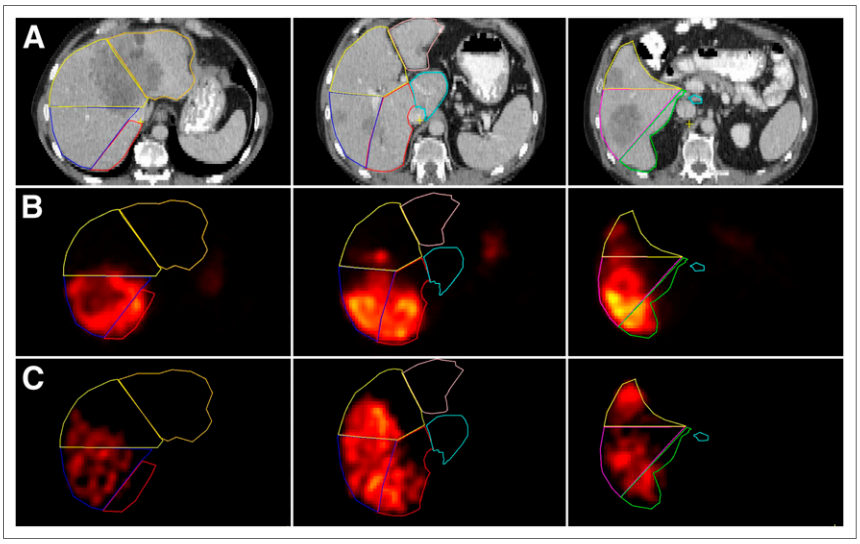

FIGURE 1. Segmentation on CT (A) and coregistration of segments on ^{99m}Tc-MAA SPECT (B) and ^{90}Y SPECT (C) after injection of activity in right hepatic artery. Clear differences in intrahepatic activity distribution are seen in this patient. There is also diffuse uptake of free pertechnetate in stomach on ^{99m}Tc-MAA SPECT, also evidenced by thyroid gland and kidney uptake (not shown).

Analysis

Contrast-enhanced CT or MR pretreatment images were used for liver segmentation according to the Bismuth adaptation of the Couinaud classification of liver anatomy (*15*). Software was developed at our institution for this purpose (Research Volumetool, version 1.3.3) (*16*). A maximum of 8 segments (volumes of interest, or VOIs) were delineated per patient. Prior liver resection and lobar procedures resulted in fewer segments. All delineated VOIs were manually registered to the ^{99m}Tc-MAA SPECT and ^{90}Y SPECT images (Fig. 1). Procedures for which coregistration was impossible or inaccurate because of differences in liver position between the different scans were excluded from analysis.

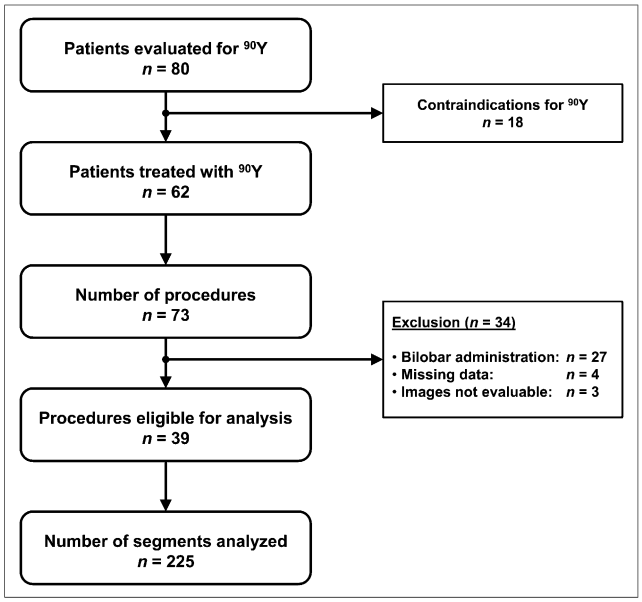

FIGURE 2. Inclusion flowchart of patient data.

The pretreatment ^{99m}Tc-MAA SPECT and the posttreatment ^{90}Y SPECT images were converted into units of ^{90}Y activity concentration by normalization of the total number of reconstructed counts in the VOIs to the total administered activity of ^{90}Y. For each VOI, this practice resulted in a predictive amount of ^{90}Y (MBq/cm^3) based on ^{99m}Tc-MAA SPECT in comparison with an actual amount of ^{90}Y based on ^{90}Y SPECT. A homogeneous distribution of the activity inside a VOI, no activity distribution outside the liver, and no interval change in liver morphology were assumed. To illustrate the clinical implications of the disagreement, a map of the absorbed dose in grays was also calculated, using a conversion factor of 49.7 Gy/(MBq/cm^3) (*17*).

The injection positions of ^{99m}Tc-MAA and ^{90}Y-microspheres were retrospectively analyzed. Three observers independently reviewed the agreement between the 2 injection positions (per procedure) on fluoroscopy images on a 4-point scale (1, very poor agreement, difference $>$ 10 mm; 2, poor agreement, difference $>$ 5–10 mm; 3, good agreement, difference $>$ 3–5 mm; 4, very good agreement, difference $<$ 3 mm). A subgroup of patients with suboptimal agreement between the injection positions (average score $\leq$ 2.5) was selected. In this subgroup, the average difference in the catheter positions as scored by 3 reviewers was 5 mm or more. The injection positions were also classified as close to a major bifurcation ($<$10 mm) or not close to a major bifurcation, and segments were classified as having $>$25% tumor involvement or $\leq$25%.

Statistical Analysis

A commercial statistical software package (SPSS for Windows, version 20.0; SPSS Inc.) was used for data analysis. Bland–Altman plots were used for evaluating agreement between pre- and posttreatment activity distributions (*18,19*). A Bland–Altman graph is the preferred method to test for agreement between 2 instruments that are intended to measure the same parameter, in our case ^{99m}Tc-MAA SPECT and ^{90}Y SPECT to measure final ^{90}Y-microsphere distribution. In a Bland–Altman plot, the difference between the 2 methods is plotted against the mean of the 2 methods. The error was estimated by the mean difference (d_m) and the SD of the differences (s). The 95% limits of agreement were calculated by $d_m \pm 2s$. Because the ^{99m}Tc-MAA was normalized to the ^{90}Y activity, the expected mean difference is zero. In Bland–Altman analysis, the width of the distribution (i.e., 95% limits of agreement) is a measurement of the agreement between the 2 methods. An absorbed dose map in grays was calculated for translation to clinical practice. Cutoff levels (10%, 20%, and 30%) for the difference from the mean were used to evaluate variability in activity distribution. The Fisher exact test was used to test differences between subgroups with differences in tumor involvement, tumor cell type, and catheter positions.

RESULTS

Eighty patients were evaluated for radioembolization (Fig. 2). In 18 patients, contraindications to therapy were found during or

TABLE 1
Baseline Characteristics

Characteristic	Data
Sex (*n*)	
Male	19
Female	12
Age (y)	
Median	60.3
Range	35–76
Primary tumor (*n*)	
Colorectal	17 (55%)
Hepatocellular	4 (13%)
Neuroendocrine	3 (10%)
Cholangiocarcinoma	2 (6%)
Other*	5 (16%)
Resin microsphere activity (MBq)	
Mean	1,002
Range	207–1,912
Liver tumor involvement (*n*)	
<25%	21 (68%)
25%–50%	9 (29%)
50%–75%	1 (3%)
75%–100%	0 (0%)
Treatment (*n*)	
Whole liver in 1 administration (1 session)	6 (19%)
Whole liver in 2 lobar administrations (2 sessions)	10 (31%)
Lobar left only	2 (6%)
Lobar right only	13 (44%)
Injection position (*n*)	
Common or proper hepatic artery	6 (15%)
Right hepatic artery	22 (57%)
Left hepatic artery	11 (28%)
Total included procedures	39
Total included liver segments	225
Segment volume (cm^3)	
Mean	320
Range	5–1,393
Previous liver-directed treatment (*n*)	
Transarterial embolization	1 (3%)
Partial liver resection	3 (10%)
Radiofrequency ablation	5 (16%)
External-beam radiotherapy	0 (0%)
Radioembolization	0 (0%)
Previous systemic treatment†	21 (68%)

*Uveal melanoma (2); pancreatic (2); unknown primary (1).

†Most patients were chemorefractory, except those with chemoresistant tumors (e.g., hepatocellular, cholangiocarcinoma, neuroendocrine, or melanoma).

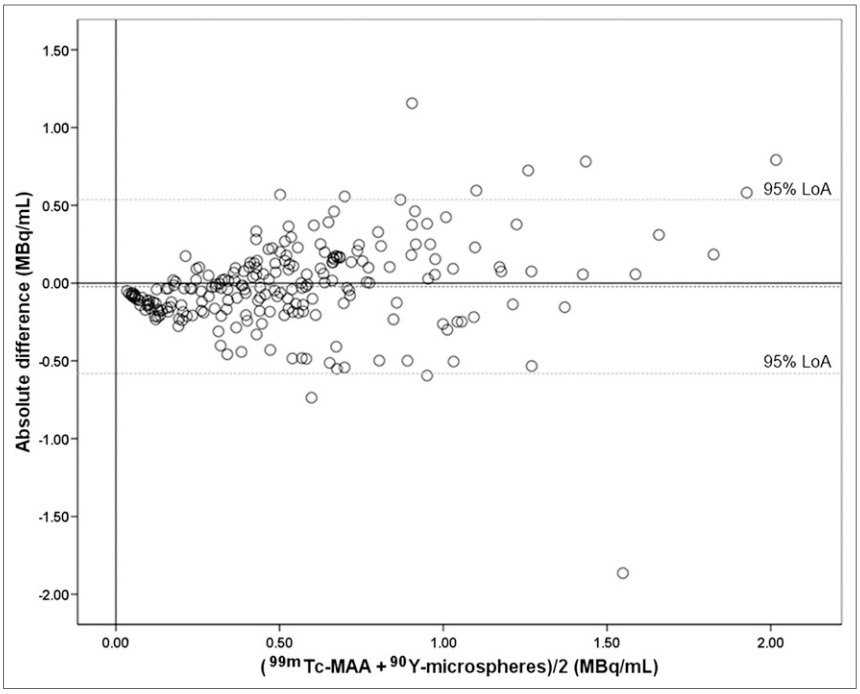

FIGURE 3. Bland–Altman plot. Difference between ^{99m}Tc-MAA and ^{90}Y-microsphere activity in each segment is plotted against mean activity in each segment. Plotted as dotted lines are 95% limits of agreement (LoA).

after the ^{99m}Tc-MAA procedure. The remaining 62 patients underwent 73 treatment procedures. Multiple injections of activity in the same procedure led to exclusion of 27 procedures, and missing data led to exclusion of 4 procedures. In another 3 procedures, technical difficulties were encountered during coregistration because of substantial differences in liver position between the different scans ($n = 2$) or because of segmentation problems ($n = 1$). In the latter patient, extensive disease in the liver made it impossible to delineate the individual liver segments. A total of 39 procedures in 31 patients were included for analysis (Table 1). The mean administered activity of ^{90}Y-microspheres was 1,002 MBq per procedure (range, 207–1,912 MBq). In 8 patients, 2 separate procedures were included, one for the left liver lobe and one for the right lobe. A total of 225 liver segments were analyzed.

The overall mean difference between pretreatment and posttreatment distribution of activity concentration for all segments was -0.022 MBq/cm^3, with an SD of the mean of 0.285 MBq/cm^3. A Bland–Altman plot was constructed with the absolute differences against their mean (Fig. 3). The 95% limits of agreement of the differences were -0.581 and 0.537 MBq/cm^3, which correspond to 95% limits of agreement of -28.9 and 26.7 Gy absorbed dose.

A difference of >10%, >20%, and >30% of the mean activity per milliliter was found in, respectively, 153 (68%), 97 (43%), and 72 (32%) of the 225 segments (Fig. 4). In every ^{99m}Tc-MAA procedure, at least 1 segment showed an under- or overestimation of >10%. A >20% and >30% difference in at least 1 segment was found for 35 (90%) and 32 (82%) of 39 procedures, respectively (Fig. 5). A substantial difference in agreement between ^{99m}Tc-MAA and ^{90}Y activity distribution was found for every procedure (Fig. 6).

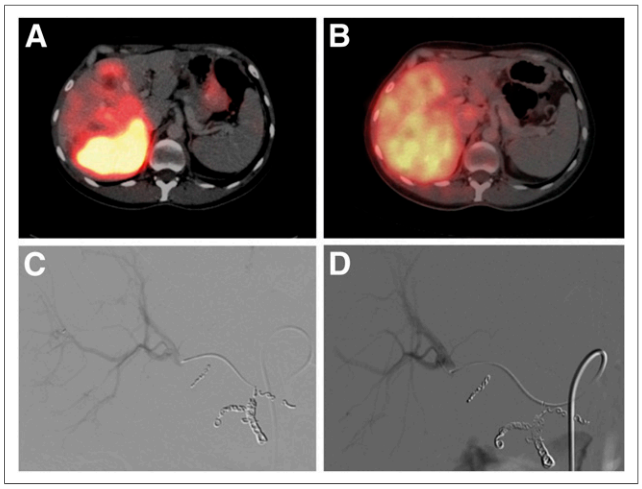

FIGURE 4. Right-sided treatment of 36-y-old patient with colorectal liver metastases. Pretreatment ^{99m}Tc-MAA SPECT images (A) show substantial distribution differences in comparison with posttreatment ^{90}Y SPECT images (B). Digital subtraction angiography images show identical position of catheter tip in right hepatic artery (C and D). Gastroduodenal artery, right gastric artery, and supraduodenal arteries were coil-embolized. Diffuse uptake of free pertechnetate in stomach on ^{99m}Tc-MAA SPECT was also seen (A).

Interestingly, the distribution differences were found to be smaller for segments with greater tumor involvement. The mean difference and 95% limits of agreement were -0.027 ± 0.603 and 0.007 ± 0.381 MBq/cm^3 for segments with ≤25% and >25% tumor involvement, respectively. In grays, the 95% limits of agreement (−18.6 to 19.3 Gy) for segments with >25% tumor involvement had a smaller width than the 95% limits of agreement for segments with ≤25% tumor involvement (−31.3 to 28.6 Gy). A relative difference of >10%, >20%, and >30% was found in, respectively, 18 (51%), 9 (26%), and 7 (20%) of the 35 segments with >25% tumor involvement and in 136 (72%), 88 (47%), and 64 (34%) of the 190 segments with ≤25% tumor involvement. This proved significant for the cutoff values of >10% ($P = 0.028$) and >20% ($P = 0.026$), but significance was not reached for a cutoff value of >30% ($P = 0.118$).

A suboptimal agreement on catheter tip position was found for 9 patients (11 procedures). The mean difference and 95% limits of agreement were -0.008 ± 0.622 MBq/cm^3 for procedures with a suboptimal agreement on catheter tip position (Fig. 7) and -0.026 ± 0.556 MBq/cm^3 for procedures with an optimal agreement on catheter tip position. A relative difference of >10%, >20%, and >30% was found in, respectively, 54 (79%), 33 (49%), and 24 (35%) of the 68 segments for procedures with a suboptimal agreement on catheter tip position and in 100 (64%), 64 (41%), and 47 (30%) of the 157 segments for procedures with an optimal agreement on catheter tip position (Fig.7). This reached

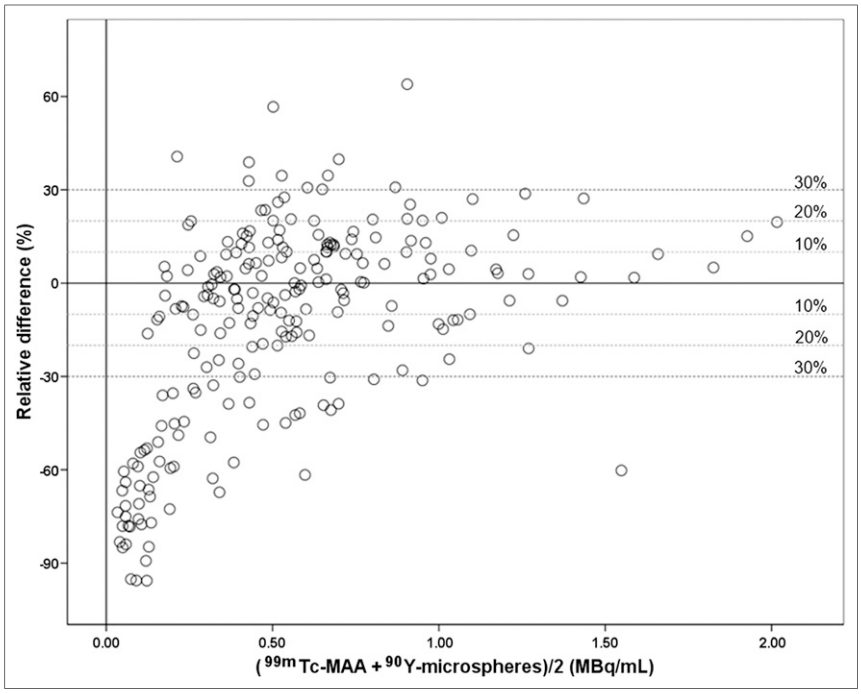

FIGURE 5. Relative difference plot. Relative difference between ^{99m}Tc-MAA and ^{90}Y-microsphere activity in percentage of mean activity is plotted against mean activity, according to Bland–Altman. Dotted lines indicate 95% limits of agreement for 3 categories representing >10%, >20%, and >30% difference in activity.

significance for the cutoff value of >10% ($P = 0.020$) but not for >20% ($P = 0.307$) and >30% ($P = 0.438$).

Significant differences were not found between procedures with the catheter tip near a major bifurcation (<10 mm) and procedures without, as long as the position was the same during the ^{99m}Tc-MAA and the ^{90}Y injection. In procedures with the catheter tip close to a major bifurcation, as well as suboptimal agreement in catheter position between the ^{99m}Tc-MAA and the ^{90}Y injection, a significant difference in activity distribution was found. A relative difference of >10%, >20%, and >30% was found in, respectively, 19 (95%), 12 (60%), and 9 (45%) of the 20 segments for procedures with these 2 characteristics, and in 133 (65%), 85 (41%), and 62 (31%) of the 205 segments for procedures without. This reached significance for the cutoff value of >10% ($P = 0.005$) but not for >20% ($P = 0.155$) and >30% ($P = 0.209$).

Evaluation of other parameters, including other combinations of parameters, did not yield any significant results. Procedures in patients with colorectal metastases (relatively hypovascular tumors) did not show any difference from procedures in patients with more hypervascular tumors, nor did treatment approach with regard to left lobar versus right lobar treatments.

DISCUSSION

It is expected that patients may greatly benefit from individualized treatment planning (*10*). Most promising in this regard is the so-called partition model. This method was previously shown to accurately predict treatment response and survival (*11,20*). The expected absorbed dose to the tumor is calculated on ^{99m}Tc-MAA SPECT. The tumors are delineated on morphologic images, whereas the dose distribution is estimated by calculation of ^{99m}Tc-MAA in the tumors, the normal liver, and the lungs. The prescribed activity may be calculated such that it does not exceed the maximum safe absorbed dose to the normal liver and lungs. Agreement between ^{99m}Tc-MAA and subsequent ^{90}Y is therefore crucial for the accuracy of the partition method.

The presented data, however, show a substantial disagreement between ^{99m}Tc-MAA and ^{90}Y activity distribution. In 68% of all segments, a difference of >10% between ^{99m}Tc-MAA and ^{90}Y activity distribution was found. In every procedure, at least 1 segment showed a >10% difference. These findings raise concern about the validity of the partition method. However, regardless of the found disagreement, early studies were able to show the accuracy of the partition method nevertheless, although dose–effect relationships with regard to toxicity on the normal liver parenchyma were ignored (*11,20*). Knowledge of the existence, the magnitude, and the etiology of disagreement between ^{99m}Tc-MAA and ^{90}Y activity distribution should ultimately lead to the improved validity of these methods. Specific technical and methodologic recommendations may help to overcome this issue.

Knesaurek et al. visually assessed the correlation between ^{99m}Tc-MAA and ^{90}Y-distribution and found that correlation could vary from poor to relatively good (voxel-based Spearman rank correlation varied from 0.451 to 0.818) (*21*). However, their methodology is questionable. Their correlations indicate that ^{90}Y activity is higher when ^{99m}Tc-MAA is higher. This does not imply that for individual measurements, the distributions are equal to (or close approximations of) each other. Agreement as described by Bland and Altman (*18*) is a more appropriate method of comparing 2 measurements of the same variable (i.e., activity distribution).

There are several factors that may have caused the disagreement in ^{99m}Tc-MAA and ^{90}Y distribution. First, difference in catheter position between the 2 procedures seems to be a key factor. Although the catheter tip was positioned at the same location, small deviations (approximately 5–10 mm) were still found. A significantly increased disagreement between ^{99m}Tc-MAA and ^{90}Y distribution was found in these procedures. In another study with more substantial differences in catheter tip position between the ^{99m}Tc-MAA and subsequent ^{90}Y procedure, investigators found that position differences ($P < 0.001$) and a catheter position close to important side branches or bifurcations ($P < 0.01$) led to significant visually assessed distribution differences between ^{99m}Tc-MAA and ^{90}Y (*12*). In the current study, we confirmed this finding quantitatively. In particular, patients with a mismatch in catheter tip position and injections close to a bifurcation showed significant disagreement. Selective administration of microspheres distal to the proper hepatic artery may largely overcome this issue. It was already shown that selective administrations are beneficial to prevent extrahepatic deposition of microsphere activity (*22*). In addition, differences in the intraluminal cross-sectional position of the catheter tip may have influenced the disagreement (Fig. 7). These

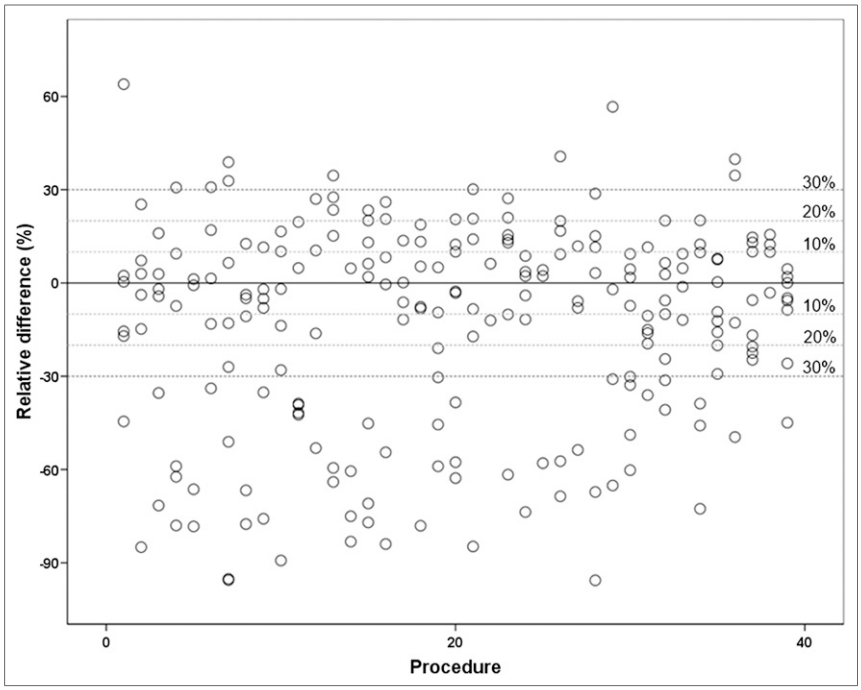

FIGURE 6. Agreement per procedure. Relative difference between ^{99m}Tc-MAA and ^{90}Y-microsphere activity for each VOI is plotted per procedure. Dotted lines indicate 95% limits of agreement for 3 categories representing >10%, >20%, and >30% difference in activity.

differences are known to cause substantial differences in preferential flow (*23–25*). Innovative catheter designs with spacers to keep the catheter tip centered in the arterial lumen during injection may lead to more comparable injection positions and subsequent improved agreement between ^{99m}Tc-MAA and ^{90}Y activity distribution (*26*).

Second, differences in the number, density, size, and morphology of the radiopharmaceuticals may also have resulted in a different activity distribution. The number of ^{99m}Tc-MAA particles (1–2 × 10^5 particles) is significantly lower than the number of ^{90}Y microspheres applied (resin: 40–80 × 10^6; glass: 1.2–8 × 10^6 particles), whereas the density of ^{99m}Tc-MAA particles (1.1 g/mL) is lower than that of ^{90}Y microspheres (resin: 1.6 g/mL; glass: 3.3 g/mL) (*27–29*). The particle size distribution of ^{99m}Tc-MAA is such that over 90% are within 10–90 μm in size (mean, 15 μm). The mean size of ^{90}Y microspheres is 32 ± 10 μm, and the morphology of the spheric ^{90}Y microspheres is also considerably different from the macroaggregated random shape of ^{99m}Tc-MAA particles (*27*). The embolization effect of the much larger number of ^{90}Y-microspheres may result in flow alterations that alter the distribution of the particles.

Third, the use of bremsstrahlung ^{90}Y SPECT after treatment leads to a degree of blurring and quantitative uncertainty. To overcome this methodologic problem, we chose to evaluate larger segment-based volumes instead of using a voxel-based analysis. The uncertainty in stochastic effects that are responsible for the measurement accuracy is far less in larger volumes. Larger VOIs were also useful to overcome quantification errors caused by coregistration artifacts. As a consequence, we were able to study quantitative distribution differences on only a segmental level. Any existing disagreement will be underestimated, since differences in certain areas of the segment may level out differences in other areas. One way to improve part of the methodology may be the use of ^{90}Y PET imaging instead of SPECT. PET facilitates more accurate quantification based on improved spatial resolution and may aid in the study of distribution on a subsegmental or tumor level (*30–32*).

And lastly, the studied population was a heterogeneous group with regard to the histopathology of the primary tumor. We could not differentiate whether histopathologic features had any influence on the results. Remarkable was the finding that a larger degree of tumor involvement was associated with a better agreement between ^{99m}Tc-MAA and ^{90}Y. This finding may be due to a lesser degree of random distribution of activity.

On one hand, the results lead to concerns about the agreement between ^{99m}Tc-MAA and ^{90}Y distribution and, consequently, the validity of activity calculation methods that are based on the assumption of agreement, such as the partition method. On the other hand, it has been shown that, although based on the false assumption of agreement, the partition method still offers huge advantages over existing methods with regard to the prediction of treatment outcome and individualized treatment planning. This may be explained by the fact that the partition method is prescribed only for patients with a limited number of hypervascular tumors. Our results show that the agreement between ^{99m}Tc-MAA and ^{90}Y

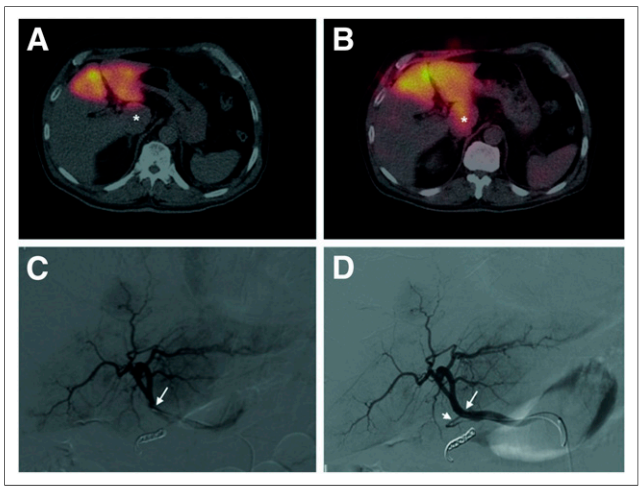

FIGURE 7. Left-sided treatment of 72-y-old patient with uveal melanoma liver metastases. Pretreatment ^{99m}Tc-MAA SPECT images (A) show substantial distribution differences in comparison with posttreatment ^{90}Y SPECT images (B), especially in caudate lobe (*). Injection position during ^{99m}Tc-MAA administration (C) and ^{90}Y administration (D) was also different. Digital subtraction angiography images show catheter tip (long arrow) positioned in left hepatic artery. At ^{90}Y administration, catheter tip was proximal to significant side branch (short arrow), probably supplying caudate lobe. Catheter was distal to this branch during ^{99m}Tc-MAA administration.

distribution in segments with a high tumor involvement is considerably better. Moreover, these patients are generally treated superselectively, beyond the major bifurcation of the proper hepatic artery, and also with fewer embolic glass microspheres. All these factors seem to contribute to a better agreement between ^{99m}Tc-MAA and ^{90}Y distribution.

On the basis of the current study, the following 2 recommendations may lead to optimization of the predictive value of a pretreatment scout dose. First, the catheter tip should be placed in exactly the same position during both procedures, possibly augmented by the use of catheters that center the tip within the lumen; second, for each administration, the catheter tip should be placed distal to major bifurcations, with selective administration in each branch to prevent preferential flow. In patients with large hypervascular tumors limited to a single lobe, the agreement between ^{99m}Tc-MAA and ^{90}Y distribution is best, but caution should be taken in patients with multiple small liver metastases in both lobes, especially when an embolic effect of the microspheres is anticipated. The latter could be the case in patients who are treated with high-dosage resin microspheres and have small livers and prior treatments with antiangiogenic drugs such as bevacizumab.

To overcome the limitations of ^{99m}Tc-MAA as a scout dose, our group has developed a new generation of microspheres for multimodality image-guided radioembolization: ^{166}Ho-poly(L-lactic acid) microspheres (*33*). The radioisotope ^{166}Ho is embedded in microspheres of poly(L-lactic acid). It emits β-radiation (half-life, 26.8 h; maximum energy, 1.77 and 1.85 MeV) and γ-radiation (γ-energy, 80.6 keV) and is paramagnetic, because the element holmium is chemically part of the lanthanide group, like gadolinium (*34–36*). The microspheres can be visualized in vivo with several clinical imaging modalities, including SPECT and MR imaging (*14,37,38*). The particles used for pretreatment evaluation and actual treatment are exactly the same, and SPECT and MR imaging are used to combine high sensitivity with high spatial-temporal resolution and superior soft-tissue contrast to optimize dosimetry before and after treatment. The performance of ^{166}Ho-microspheres as a scout dose to predict distribution of the therapy dose is currently under investigation.

CONCLUSION

Individualized treatment planning methods may be used for optimized safety and efficacy of radioembolization treatments. By definition, these methods are based on predictive scout dose distribution within the target volume. The limited agreement between ^{99m}Tc-MAA and ^{90}Y distribution in current clinical practice raises concern about the validity of these methods. Care should be taken to use proper administration techniques to overcome this limitation.

DISCLOSURE

The costs of publication of this article were defrayed in part by the payment of page charges. Therefore, and solely to indicate this fact, this article is hereby marked "advertisement" in accordance with 18 USC section 1734. No potential conflict of interest relevant to this article was reported.

REFERENCES

1. Kennedy A, Coldwell D, Sangro B, Wasan H, Salem R. Radioembolization for the treatment of liver tumors: general principles. *Am J Clin Oncol.* 2012;35:91–99.
2. Sangro B, Salem R, Kennedy A, Coldwell D, Wasan H. Radioembolization for hepatocellular carcinoma: a review of the evidence and treatment recommendations. *Am J Clin Oncol.* 2011;34:422–431.
3. Coldwell D, Sangro B, Salem R, Wasan H, Kennedy A. Radioembolization in the treatment of unresectable liver tumors: experience across a range of primary cancers. *Am J Clin Oncol.* 2012;35:167–177.
4. Lewandowski RJ, Sato KT, Atassi B, et al. Radioembolization with ^{90}Y microspheres: angiographic and technical considerations. *Cardiovasc Intervent Radiol.* 2007;30:571–592.
5. Dezarn WA, Cessna JT, DeWerd LA, et al. Recommendations of the American Association of Physicists in Medicine on dosimetry, imaging, and quality assurance procedures for ^{90}Y microsphere brachytherapy in the treatment of hepatic malignancies. *Med Phys.* 2011;38:4824–4845.
6. Lenoir L, Edeline J, Rolland Y, et al. Usefulness and pitfalls of MAA SPECT/CT in identifying digestive extrahepatic uptake when planning liver radioembolization. *Eur J Nucl Med Mol Imaging.* 2012;39:872–880.
7. Ho S, Lau WY, Leung TW, et al. Partition model for estimating radiation doses from yttrium-90 microspheres in treating hepatic tumours. *Eur J Nucl Med.* 1996;23:947–952.
8. Ho S, Lau WY, Leung TW, et al. Tumour-to-normal uptake ratio of ^{90}Y microspheres in hepatic cancer assessed with 99Tcm macroaggregated albumin. *Br J Radiol.* 1997;70:823–828.
9. Ho S, Lau WY, Leung TW, Chan M, Johnson PJ, Li AK. Clinical evaluation of the partition model for estimating radiation doses from yttrium-90 microspheres in the treatment of hepatic cancer. *Eur J Nucl Med.* 1997;24:293–298.
10. Lau WY, Kennedy AS, Kim YH, et al. Patient selection and activity planning guide for selective internal radiotherapy with yttrium-90 resin microspheres. *Int J Radiat Oncol Biol Phys.* 2012;82:401–407.
11. Kao YH, Hock Tan AE, Burgmans MC, et al. Image-guided personalized predictive dosimetry by artery-specific SPECT/CT partition modeling for safe and effective ^{90}Y radioembolization. *J Nucl Med.* 2012;53:559–566.
12. Jiang M, Fischman A, Nowakowski FS, et al. Segmental perfusion differences on paired tc-99m macroaggregated albumin (MAA) hepatic perfusion imaging and yttrium-90 (Y-90) bremsstrahlung imaging studies in SIR-sphere radioembolization: associations with angiography. *J Nucl Med Radiat Ther.* 2012;3:122.
13. Kennedy A, Nag S, Salem R, et al. Recommendations for radioembolization of hepatic malignancies using yttrium-90 microsphere brachytherapy: a consensus panel report from the radioembolization brachytherapy oncology consortium. *Int J Radiat Oncol Biol Phys.* 2007;68:13–23.
14. Elschot M, Nijsen JF, Dam AJ, de Jong HW. Quantitative evaluation of scintillation camera imaging characteristics of isotopes used in liver radioembolization. *PLoS ONE.* 2011;6:e26174.
15. Bismuth H. Surgical anatomy and anatomical surgery of the liver. *World J Surg.* 1982;6:3–9.
16. Bol GH, Kotte AN, van der Heide UA, Lagendijk JJ. Simultaneous multimodality ROI delineation in clinical practice. *Comput Methods Programs Biomed.* 2009;96:133–140.
17. Gulec SA, Mesoloras G, Stabin M. Dosimetric techniques in ^{90}Y-microsphere therapy of liver cancer: the MIRD equations for dose calculations. *J Nucl Med.* 2006;47:1209–1211.
18. Bland JM, Altman DG. Statistical methods for assessing agreement between two methods of clinical measurement. *Lancet.* 1986;1:307–310.
19. Bland JM, Altman DG. Comparing methods of measurement: why plotting difference against standard method is misleading. *Lancet.* 1995;346:1085–1087.
20. Garin E, Lenoir L, Rolland Y, et al. Dosimetry based on ^{99m}Tc-macroaggregated albumin SPECT/CT accurately predicts tumor response and survival in hepatocellular carcinoma patients treated with ^{90}Y-loaded glass microspheres: preliminary results. *J Nucl Med.* 2012;53:255–263.
21. Knesaurek K, Machac J, Muzinic M, DaCosta M, Zhang Z, Heiba S. Quantitative comparison of yttrium-90 (^{90}Y)-microspheres and technetium-99m (^{99m}Tc)-macroaggregated albumin SPECT images for planning ^{90}Y therapy of liver cancer. *Technol Cancer Res Treat.* 2010;9:253–262.
22. Barentsz MW, Vente MA, Lam MG, et al. Technical solutions to ensure safe yttrium-90 radioembolization in patients with initial extrahepatic deposition of ^{99m}technetium-albumin macroaggregates. *Cardiovasc Intervent Radiol.* 2011;34:1074–1079.
23. Kao YH, Tan EH, Teo TK, Ng CE, Goh SW. Imaging discordance between hepatic angiography versus Tc-99m-MAA SPECT/CT: a case series, technical discussion and clinical implications. *Ann Nucl Med.* 2011;25:669–676.
24. Kennedy AS, Kleinstreuer C, Basciano CA, Dezarn WA. Computer modeling of yttrium-90-microsphere transport in the hepatic arterial tree to improve clinical outcomes. *Int J Radiat Oncol Biol Phys.* 2010;76:631–637.
25. Basciano CA, Kleinstreuer C, Kennedy AS, Dezarn WA, Childress E. Computer modeling of controlled microsphere release and targeting in a representative hepatic artery system. *Ann Biomed Eng.* 2010;38:1862–1879.

26. Rose SC, Kikolski SG, Chomas JE. Downstream hepatic arterial blood pressure changes caused by deployment of the Surefire AntiReflux expandable tip. *Cardiovasc Intervent Radiol.* December 19, 2012 [Epub ahead of print].
27. Bult W, Vente MA, Zonnenberg BA, Van Het Schip AD, Nijsen JF. Microsphere radioembolization of liver malignancies: current developments. *Q J Nucl Med Mol Imaging.* 2009;53:325–335.
28. SIR-Spheres Yttrium-90 Resin Microspheres [package insert]. Woburn, MA: Sirtex Medical Inc.; 2013.
29. Lewandowski RJ, Riaz A, Ryu RK, et al. Optimization of radioembolic effect with extended-shelf-life yttrium-90 microspheres: results from a pilot study. *J Vasc Interv Radiol.* 2009;20:1557–1563.
30. Lhommel R, van Elmbt L, Goffette P, et al. Feasibility of ^{90}Y TOF PET-based dosimetry in liver metastasis therapy using SIR-Spheres. *Eur J Nucl Med Mol Imaging.* 2010;37:1654–1662.
31. Gates VL, Esmail AA, Marshall K, Spies S, Salem R. Internal pair production of ^{90}Y permits hepatic localization of microspheres using routine PET: proof of concept. *J Nucl Med.* 2011;52:72–76.
32. Kao YH, Tan EH, Ng CE, Goh SW. Yttrium-90 time-of-flight PET/CT is superior to Bremsstrahlung SPECT/CT for postradioembolization imaging of microsphere biodistribution. *Clin Nucl Med.* 2011;36:e186–e187.
33. Smits ML, Nijsen JF, van den Bosch MA, et al. Holmium-166 radioembolisation in patients with unresectable, chemorefractory liver metastases (HEPAR trial): a phase 1, dose-escalation study. *Lancet Oncol.* 2012;13:1025–1034.
34. Nijsen JF, Zonnenberg BA, Woittiez JR, et al. Holmium-166 poly lactic acid microspheres applicable for intra-arterial radionuclide therapy of hepatic malignancies: effects of preparation and neutron activation techniques. *Eur J Nucl Med Mol Imaging.* 1999;26:699–704.
35. Zielhuis SW, Nijsen JF, Seppenwoolde JH, et al. Lanthanide bearing microparticulate systems for multi-modality imaging and targeted therapy of cancer. *Curr Med Chem Anticancer Agents.* 2005;5:303–313.
36. Zielhuis SW, Nijsen JF, de Roos R, et al. Production of GMP-grade radioactive holmium loaded poly(L-lactic acid) microspheres for clinical application. *Int J Pharm.* 2006;311:69–74.
37. Seevinck PR, Seppenwoolde JH, de Wit TC, et al. Factors affecting the sensitivity and detection limits of MR imaging, CT, and SPECT for multimodal diagnostic and therapeutic agents. *Anticancer Agents Med Chem.* 2007;7:317–334.
38. van de Maat GH, Seevinck PR, Elschot M, et al. MR imaging-based biodistribution assessment of holmium-166 poly(L-lactic acid) microspheres after radioembolisation. *Eur Radiol.* 2013;23:827–835.